Eur. Phys. J. C 34, 335–344 (2004)
Digital Object Identifier (DOI) 10.1140/epjc/s2004-01724-6

THE EUROPEAN PHYSICAL JOURNAL C

$K\overline{K}$ photoproduction and S–P-wave interference

Ł. Bibrzycki[1], L. Leśniak[1], A.P. Szczepaniak[2]

[1] Department of Theoretical Physics, The Henryk Niewodniczański Institute of Nuclear Physics, Polish Academy of Sciences, 31-342 Kraków, Poland
[2] Physics Department and Nuclear Theory Center, Indiana University, Bloomington, IN 47405, USA

Received: 28 August 2003 / Revised version: 3 February 2004 /
Published online: 23 March 2004 –

Abstract. Results of a new analysis of the K^+K^- photoproduction at two photon energies, $E_\gamma = 4\,\mathrm{GeV}$ and 5.65 GeV, with a particular emphasis on the S-wave production are presented. We show that the proper treatment of all the helicity components of the S- and P-waves enables one to eliminate the reported discrepancies in the extraction of the S-wave photoproduction cross section from the experimental data.

1 Introduction

From the early days of QCD, light meson spectroscopy played an important role in the development of the theory and in the understanding of its low energy structure. The flavour symmetry of QCD originates in part from the observed $SU(3)$ multiplet structure of the light pseudoscalar and vector mesons. More recently, scalar and tensor spectra have provided evidence for a possible over-population of the $Q\overline{Q}$ spectrum and for the existence of gluon-rich states [1–4]. The possible existence of gluonic excitations is one of the most intriguing features of meson spectroscopy. There is tantalizing evidence of exotic, hybrid mesons in the spectrum around 1.6 GeV [5–7], and future experiments proposed for JLab and GSI in the light and charm sector respectively will map out the exotic spectrum. The glueball signature comes primarily from the analysis of the Crystal Barrel $p\bar{p}$ and WA102 central production data [1, 3]. Detailed mapping of various scalar meson decay channels led to the identification of $f_0(1370)$, $f_0(1500)$ and $f_0(1710)$ states, all expected to contain significant gluon components. While the genuine QCD resonances in the scalar channel are not expected to occur below 1 GeV, the low energy region can be studied using standard, low energy expansion techniques. These include the effective range expansion, N/D and other methods based on analyticity coupled with truncation of the unitarity condition. The parameters of the soft meson–meson interactions, e.g. subtraction constants, form factors, coupling strengths etc., effectively correspond to local potentials smeared over distance scales of the orders of $\sim 1\,\mathrm{fm}$, i.e. close to the pion root mean square radii. The strength of the interaction can be constrained from chiral symmetry or simply fitted to the data [8–11]. As a result one obtains a very good description of the spectrum including the resonance region. Furthermore, the behavior of the scattering amplitude in the complex energy plane enables one to establish the existence of dynamical resonances such as the isoscalar $\sigma(600)$ and $f_0(980)$ and the isovector $a_0(980)$ mesons. The last two are particularly interesting as they are very sensitive to the details of the meson–meson interactions. This is due to the proximity of the $K\overline{K}$ threshold. In particular the detailed structure of the $f_0(980)$, e.g., whether it is a genuine bound state or a virtual bound state, strongly depends on the threshold $K\overline{K}$ interaction parameters. Since the $K\overline{K}$ channel also influences the higher mass region, a proper description of its dynamics is crucial for a partial wave analysis and the identification of exotic, hybrid or glueball signals. Furthermore the $K\overline{K}$ system is relevant for testing the origins of CP violation and possible signals of CPT violation via hadronic interferometry [12].

The data on the near threshold $K\overline{K}$ production are very scarce and come mainly from high energy peripheral production [13, 14]. In the medium energy region, $E_\gamma^{\mathrm{lab}} \sim$ a few GeV, it is advantageous to study the $K\overline{K}$ system in photoproduction. A real photon couples strongly to vector mesons and near the $K\overline{K}$ threshold ϕ photoproduction dominates the $K\overline{K}$ spectrum. In this energy range the ϕ photoproduction cross section is large, $\sigma(\gamma P \to \phi p) \sim 0.5\,\mu\mathrm{b}$, and has an energy dependence characteristic for diffraction. The s-channel baryon resonance production cross section is highly suppressed at these energies, and the t-channel meson exchange (π) is marginally relevant only at E_γ very close to threshold [15]. Finally, the S-wave $K\overline{K}$ state, dominated in this mass range by the $f_0(980)$ in the isoscalar and by the $a_0(980)$ in the isovector channel, can be accessed via interference with the ϕ meson in the P-wave. This S–P interference was first explored in experiments at DESY [16, 17] and Daresbury [18], and could be further studied with high statistics at an energy upgraded JLab.

In the analysis of the data from the DESY and Daresbury experiments, however, the rich spectrum of the S-wave $K\overline{K}$ has not been fully explored. In both cases the

S-wave was parameterized as either a simple Breit–Wigner resonance or a non-resonant background. The two analyses yielded results for the S-wave production cross section different from each other by more than one order of magnitude. Finally, apart from the K^+K^- mass spectrum, only one moment, $\langle Y_0^1 \rangle$, describing the K^+ angular distribution, has been analyzed and very simplified assumptions about the nucleon spin dependence have been made.

In this paper we use the results of a recent calculation of the coupled channel scalar–isoscalar and scalar–isovector spectra together with a diffractive model for P-wave production to interpret the existing S–P interference data and estimate the S-wave production cross section with a better accuracy than in the phenomenological analyses already published in [16–18]. Here we shall discuss a complete set of six moments $\langle Y_M^L \rangle$ of spherical harmonics including $L = 0$ and $L = 1$. In the following section we shall present the theoretical foundation of the S- and P-wave photoproduction and discuss the main features of the existing data. In Sect. 3 we present results of the numerical analysis and fits to the data. Conclusions and an outlook are given in Sect. 4.

2 S- and P-wave photoproduction

In this paper we consider the unpolarized $K\overline{K}$ photoproduction reaction

$$\gamma p \to K^+K^-p\,, \tag{1}$$

for incident photon laboratory energies E_γ of the order of a few GeV. This is an optimum energy range for the S-wave $K\overline{K}$ production. In this energy range the process is dominated by pomeron exchange, leading to ϕ meson production which becomes even more important as the photon energy increases. However, t-channel processes, expected to be responsible for the S-wave production, decrease rapidly with energy. The experimental evidence for the S–P interference in the E_γ range between 2.8 and 6.7 GeV was presented in [16–18]. The values of the S-wave photoproduction cross sections found in these experimental analyses varied between 2.7 and 96 nb. In both cases, in the effective mass range $1.00\,\mathrm{GeV} < M_{K\overline{K}} < 1.04\,\mathrm{GeV}$, in the rest frame of the $K\overline{K}$ system an asymmetry in the kaon polar angle distribution was observed. This can only be the case if there are odd powers of $\cos\theta$ in the angular distribution. For low partial waves this implies the presence of both S- and P-waves. This feature of the angular distribution is independent of the magnetic-quantum number, i.e. the choice of the quantization axis. Due to the empirical s-channel helicity conservation, diffractive production is most naturally analyzed in the s-channel helicity frame, which in our case corresponds to the rest frame of the $K\overline{K}$ pair with the z-axis anti-parallel to the direction of the recoiling nucleon. In another reference frame, called the t-channel frame or the Gottfried–Jackson frame, the z-axis is chosen along the direction of the photon beam with the $K\overline{K}$ pair at rest [19]. In both cases the y-axis is perpendicular to the production plane.

As discussed in [20], in this energy range, the S-wave production is expected to be dominated by vector ρ, ω and pseudoscalar π, K t-channel exchanges.

As a function of the momentum transfer squared t, the kaon pair invariant mass $M_{K\overline{K}}$ and the K^+ decay angles $\Omega = (\theta, \phi)$ in the s-channel frame the photoproduction amplitude restricted to S- and P-waves can be written as

$$T_{\lambda_\gamma \lambda \lambda'}(t, M_{K\overline{K}}, \Omega) = \sum_{L=S,P;M} T^L_{\lambda_\gamma \lambda \lambda' M}(t, M_{K\overline{K}})\; Y^L_M(\Omega)\,. \tag{2}$$

Here λ_γ, λ and λ' denote the photon, target proton and recoil proton helicities, respectively, and $Y^L_M(\Omega)$ are the spherical harmonics. The corresponding four-momenta will be denoted by q, p, p', and k_1 and k_2 will be used for the K^+ and the K^- momenta, respectively. The unpolarized differential cross section is given by

$$\frac{\mathrm{d}\sigma}{\mathrm{d}t\;\mathrm{d}M_{K\overline{K}}\;\mathrm{d}\Omega} = \frac{\kappa_f}{32\;(2\pi)^3\;m_p^2\;E_\gamma^2}\frac{1}{4}\sum_{\lambda_\gamma\lambda\lambda'}|T_{\lambda_\gamma\lambda\lambda'}(t, M_{K\overline{K}}, \Omega)|^2\,, \tag{3}$$

where m_p is the proton mass, m_K is the kaon mass and $\kappa_f = \sqrt{\frac{M^2_{K\overline{K}}}{4} - m_K^2}$ is the kaon momentum in the rest system of the $K\overline{K}$ pair. The S-wave amplitude T^S and the P-wave amplitude T^P have been described in [20,21], respectively. Here we will briefly summarize the basic properties of these amplitudes. The S-wave $K\overline{K}$ production is parameterized as a double t-channel exchange. In the upper meson vertex we use a simple meson exchange and allow for an interaction of the two produced mesons in the final state. The dominant exchanges for the S-wave $K\overline{K}$ production are shown in Fig. 1. At the nucleon vertex we use either normal or Regge propagators of the exchanged vector mesons. The normal propagator of the vector meson of the mass m_e is equal to $(t - m_e^2)^{-1}$ and the Regge type propagator reads

$$-[1 - \mathrm{e}^{-\mathrm{i}\pi\alpha(t)}]\;\Gamma(1 - \alpha(t))\;(\alpha' s)^{\alpha(t)}/(2s^{\alpha_0})\,, \tag{4}$$

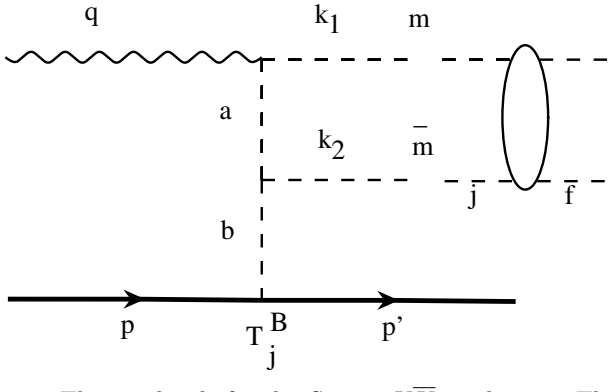

Fig. 1. The amplitude for the S-wave $K\overline{K}$ production. The a in the Born amplitude T_j^{B} stands for π, K, ρ and ω mesons, the b stands for ρ or ω mesons and $m\overline{m}$ denotes either a $\pi\pi$ or $K\overline{K}$ pair. The oval represents the final state rescattering amplitude

where we have the vector meson trajectory $\alpha(t) = \alpha_0 + \alpha'(t - m_e^2)$, $\alpha_0 = 1$ and $\alpha' = 0.9\,\mathrm{GeV}^{-2}$. The final state interactions include the $\pi\pi$ and $K\overline{K}$ channels. Both interactions can have a resonant character. This is important since the S-wave in the mass region of interest, $M_{K\overline{K}} \sim 1\,\mathrm{GeV}$, is dominated by the $f_0(980)$ and $a_0(980)$ resonances. We should notice that the K^+K^- system is an equal mixture of the isospin 0 and isospin 1 states. The isoscalar $f_0(980)$ resonance has a main branching to $\pi\pi$ and in addition an important coupling to $K\overline{K}$. The isovector $a_0(980)$ resonance lies also very close to the $K\overline{K}$ threshold so one should take it into account in the calculations of the final state interactions. The S-wave K^+K^- photoproduction amplitude T_f^S can therefore be written as

$$T^S_{\lambda_\gamma\lambda\lambda'} = \bar{u}(p',\lambda')J^S_\mu(p',p,q,M_{K\overline{K}})\epsilon^\mu(q,\lambda_\gamma)u(p,\lambda) \quad (5)$$

and decomposed as $T_f^S = \frac{1}{2}[T_f^S(I=0)+T_f^S(I=1)]$. Here ϵ is the photon helicity four-vector and J_μ^S is the S-wave projection of the appropriate current operator. As illustrated in Fig. 1 each S-wave amplitude is a sum of products of the Born amplitudes $T_j^{\mathrm{B}}(I)$ describing the t-channel meson or Regge exchanges and the final state interaction factors $F_{jf}(I)$:

$$T_f^S(I) = \sum_{j=\pi\pi,K\overline{K}} T_j^{\mathrm{B}}(I)F_{jf}(I)\,. \quad (6)$$

If we restrict ourselves to the on-shell part of the final state coupled channel interactions, represented by the 2×2 S-matrix elements S_{jf}^I, then the factors $F_{jf}(I)$ can be written as

$$F_{jf}(I) = \frac{1}{2}(\delta_{jf} + S^I_{jf})\sqrt{\frac{\kappa_j}{\kappa_f}}\,, \quad (7)$$

where $\kappa_j = \sqrt{\frac{M^2_{m\overline{m}}}{4} - m_j^2}$ and $M_{m\overline{m}}$ is the effective mass of the $m\overline{m}$ pion or kaon pair and m_j is the pion or kaon mass. The explicit forms of the S-wave Born amplitudes T_j^{B} are given in [20]. The magnitude of the off-shell part of the final state interaction amplitude is much less certain than the on-shell part as has been shown in [20]. Thus we prefer here to use only the on-shell part of the amplitude and correct it later by a constant modification factor. In comparison with [20] we have added in these amplitudes a t-dependent factor $\exp(B_S t)$, where the parameter $B_S = 1.07\,\mathrm{GeV}^{-2}$ is responsible for a spatial dimension of the meson (kaon or pion) coupled to the photon. In [20] the meson in the upper vertex in Fig. 1 was treated as a point-like particle. The isoscalar S^I_{jf}-matrix elements can be expressed by the scalar–isoscalar phase shifts δ and the inelasticity η in the two channels $\pi\pi$ and $K\overline{K}$:

$$S^{I=0}_{jf} = \begin{pmatrix} \eta e^{2i\delta^{I=0}_{\pi\pi}} & i\sqrt{1-\eta^2}e^{i(\delta^{I=0}_{\pi\pi}+\delta^{I=0}_{K\overline{K}})} \\ i\sqrt{1-\eta^2}e^{i(\delta^{I=0}_{\pi\pi}+\delta^{I=0}_{K\overline{K}})} & \eta e^{2i\delta^{I=0}_{K\overline{K}}} \end{pmatrix}. \quad (8)$$

These elements have been computed in [22] and here we use the solution A, corresponding to the so-called "down-flat" data of the phase shift analysis [23].

The $I = 1$ $K\overline{K}$ interaction near 1 GeV is very strongly influenced by the $a_0(980)$ resonance which decays dominantly into the $\pi\eta$. A coupled channel model including the $\pi\eta$ and $K\overline{K}$ states has been formulated in [24] and recently compared to the existing data [25]. As a result one obtains the $K\overline{K}$ scalar–isovector S-matrix elements $S^{I=1}_{jf}$ which differ from the scalar–isoscalar S-matrix elements written in (8). This new information has been incorporated into calculations of the final state K^+K^- interactions.

The P-wave amplitudes corresponding to a given projection M of the K^+K^- angular momentum on the quantization axis can be handled in a similar way as the S-wave, i.e. we write

$$T^P_{\lambda_\gamma\lambda\lambda' M} = \bar{u}(p',\lambda')\; J^P_{\mu M}(p,p',q,M_{K\overline{K}})\;\epsilon^\mu(q,\lambda_\gamma)\;u(p,\lambda)\,, \quad (9)$$

with $J^P_{\mu M}$ being the P-wave projection of the current. The P-wave current is described in detail in [21]. In particular, it is saturated by diffractive ϕ meson production,

$$J_\mu = \frac{\mathrm{i}\;F(t)}{M_\phi^2 - M^2_{K\overline{K}} - \mathrm{i}M_\phi\Gamma_\phi} \times [\gamma^\nu q_\nu(k_1-k_2)^\mu - q^\nu(k_1-k_2)_\nu\gamma^\mu]\,, \quad (10)$$

where γ^μ are the Dirac matrices, and M_ϕ and Γ_ϕ are ϕ mass and width, respectively. The Lorentz–Dirac structure of the current is motivated by the Donnachie–Landshoff model for the pomeron exchange which assumes vector coupling of the pomeron to hadrons [26]. The two terms in (10) are needed to preserve electromagnetic current conservation, $q^\mu J_\mu = 0$. One can show that $q^\mu J^P_{\mu M} = 0$ is satisfied independently by each projection of the $K\overline{K}$ spin, $M = \pm1, 0$. Then in the phenomenological analysis of the data one can separately modify different $J^P_{\mu M}$ components by multiplying them by constant factors. The function $F(t)$ is a phenomenological function which will be suitably parameterized to reproduce, at fixed energy, the t-dependence of the observed ϕ photoproduction. Its analytical form will be specified in the next section. We note, however, that this model for the P-wave does not lead to significant suppression of the single helicity flip amplitude. In particular in the high energy limit of $s \simeq 2E_\gamma m_p \gg |t|$ and $s \gg M_{K\overline{K}}$ the helicity non-flip, single-flip and double-flip amplitudes with $\lambda_\gamma = 1$ behave as

$$T_{1\lambda'\lambda1} \propto 2N_{\lambda'\lambda}M_{K\overline{K}}\,,$$
$$T_{1\lambda'\lambda0} \propto N_{\lambda'\lambda}\sqrt{-2t}\,, \quad T_{1\lambda'\lambda-1} \to O(1/s)\,, \quad (11)$$

respectively. The proportionality constant $N_{\lambda'\lambda}$ contains the Breit–Wigner propagator of (10) and is finite as $t' = t - t_{\min} \to 0$. The diagonal elements of the matrix N are finite and the off-diagonal ones, corresponding to nucleon helicity flip, are $O(1/s)$. Thus the only suppression of the photon–meson coupling comes from the angular momentum conservation factor $t^{|\lambda_\gamma - M|/2}$, but it is otherwise finite at high energy. The existing data on ϕ photoproduction suggest that the helicity flip amplitude is of the order of 10% of

the dominant, helicity non-flip one at photon energies below 10 GeV [18]. Thus, qualitatively the model has the correct features, but the quantitative agreement may require adjusting the normalization and the phase of the helicity flip amplitudes. This can be done by multiplication of these amplitudes by a constant complex factor $C_{10}\ \exp(\mathrm{i}\phi_{10})$, where C_{10} is a real positive number and ϕ_{10} is an additional phase of the P-wave amplitude with $M = 0$. We will not modify the phases of the dominant helicity non-flip amplitudes; however, we do change slightly their moduli as well as the moduli of small double helicity flip amplitudes to keep the total P-wave cross section untouched. The phases of the small double helicity flip amplitudes are the same as the phases of the corresponding non-flip amplitudes. Similarly, for the S-wave amplitudes we introduce a constant modification factor equal to $C_{00}\ \exp(\mathrm{i}\phi_{00})$. It is assumed that the parameters $C_{10}, \phi_{10}, C_{00}$ and ϕ_{00} do not depend on the proton helicities λ nor λ'. The experimental data on the angular distribution of the $K\overline{K}$ pair are given in terms of the moments $\langle Y_M^L \rangle$ of the angular distribution evaluated in the s-channel helicity frame,

$$\langle Y_M^L \rangle \equiv \int_{t_1}^{t_2} \mathrm{d}t \int \mathrm{d}\Omega\ Y_M^L(\Omega) \frac{\mathrm{d}\sigma}{\mathrm{d}t\ \mathrm{d}M_{K\overline{K}}\ \mathrm{d}\Omega} = \mathcal{N} \int\int \mathrm{d}t\ \mathrm{d}\Omega \sum_{\lambda_\gamma \lambda \lambda'} |T_{\lambda_\gamma \lambda \lambda'}|^2 Y_M^L(\Omega)\,, \quad (12)$$

where $\mathcal{N}$ takes into account the photon flux and the 1/4 factor standing before the sum in (3). The lowest moment is normalized to the K^+K^- mass distribution integrated over the momentum transfer squared range limited by t_1 and t_2:

$$\langle Y_0^0 \rangle = \frac{1}{\sqrt{4\pi}} \frac{\mathrm{d}\sigma}{\mathrm{d}M_{K\overline{K}}}\,. \quad (13)$$

In terms of the S- and P-partial waves, the non-vanishing moments are given by

$$\begin{aligned}
\langle Y_0^0 \rangle &= \frac{\mathcal{N}}{\sqrt{4\pi}} \left(|S|^2 + |P_+^2| + |P_-^2| + |P_0^2| \right)\,, \\
\langle Y_0^1 \rangle &= \frac{\mathcal{N}}{\sqrt{4\pi}} \left(S P_0^* + S^* P_0 \right)\,, \\
\langle Y_1^1 \rangle &= \frac{\mathcal{N}}{\sqrt{4\pi}} \left(P_+ S^* - S P_-^* \right)\,, \\
\langle Y_0^2 \rangle &= \frac{\mathcal{N}}{\sqrt{4\pi}} \sqrt{\frac{1}{5}} \left(2 P_0 P_0^* - P_+ P_+^* - P_- P_-^* \right)\,, \\
\langle Y_1^2 \rangle &= \frac{\mathcal{N}}{\sqrt{4\pi}} \sqrt{\frac{3}{5}} \left(P_+ P_0^* - P_0 P_-^* \right)\,, \\
\langle Y_2^2 \rangle &= \frac{\mathcal{N}}{\sqrt{4\pi}} \sqrt{\frac{6}{5}} \left(-P_+ P_-^* \right)\,. \quad (14)
\end{aligned}$$

Here S, P stand for T^S and T^P amplitudes, respectively, and summation over photon and nucleon spin indices is implicit, e.g.,

$$P_+ P_0^* = \sum_{\lambda_\gamma \lambda \lambda'} T^P_{\lambda_\gamma \lambda \lambda' 1}\ T^{*P}_{\lambda_\gamma \lambda \lambda' 0}\,. \quad (15)$$

The dominant P_+- and P_--waves originating from $M = \lambda_\gamma = +1$ and $M = \lambda_\gamma = -1$ helicity non-flip production will manifest themselves in a large, positive $\langle Y_0^0 \rangle$ and a large negative $\langle Y_0^2 \rangle$ near $M_{K\overline{K}} = 1.02\,\mathrm{GeV}$ – the mass of the ϕ resonance. This is indeed the dominant feature of the data as shown in Figs. 3 and 4. Since $|S|^2 \ll |P_\pm|^2$ the S-wave is not expected to be significant in the mass spectrum i.e. in the $\langle Y_0^0 \rangle$ moment. It will primarily contribute to the $\cos\theta$ asymmetry measured by the $\langle Y_0^1 \rangle$ and the $\langle Y_1^1 \rangle$ moments. For diffractive P-wave production with equal phases of all P amplitudes, it is expected that $|\langle Y_1^1 \rangle| > |\langle Y_0^1 \rangle|$, since the latter describes the interference between the S- and the helicity flip P_0-wave which has a smaller magnitude than the P_+ one. The data suggest, however, that the two moments are comparable with more structure actually seen in the $\langle Y_0^1 \rangle$ moment. This can only be possible if we allow a well defined pattern of phases to occur in the three waves. This justifies our choice of additional parameters as already described above. In the following section we discuss the results of fitting this model to the experimental data.

3 Numerical results

In the analysis of the S- and P-wave production we compare the model described above to the t, $M_{K\overline{K}}$ and the angular distribution of the $K\overline{K}$ system at two photon energies, $E_\gamma = 4\,\mathrm{GeV}$ [18] and $E_\gamma = 5.65\,\mathrm{GeV}$ [16, 17]. The two photon energies represent averages of the photon beam energies used in the experiments performed at Daresbury and at DESY, respectively. At first we discuss the momentum transfer dependence of the cross section integrated over the $K\overline{K}$ effective mass and the kaon emission angles.

3.1 Momentum transfer distributions and integrated cross sections at $E_\gamma = 4\,\mathrm{GeV}$

At 4 GeV photon energy the comparison between the experimentally measured differential cross section $\mathrm{d}\sigma/\mathrm{d}t$ and the model cross section integrated over the $K\overline{K}$ mass $0.997\,\mathrm{GeV} < M_{K\overline{K}} < 1.042\,\mathrm{GeV}$ is shown in Fig. 2. For this comparison, the t-dependent normalization $F(t)$ in the P-wave was chosen as

$$F(t) = \frac{D_1 \mathrm{e}^{bt}}{(1 - t/a)^2}\,, \quad (16)$$

where the normalization constant D_1 has been adjusted to reproduce the very forward value of $\mathrm{d}\sigma/\mathrm{d}t\ (t_0) = 1.852\,\mu\mathrm{b/GeV}^2$ at small argument, $t_0 = -0.0225\,\mathrm{GeV}^2$, and the remaining parameters have been chosen as $a = 0.7\,\mathrm{GeV}^2$ and $b = 0.05\,\mathrm{GeV}^{-2}$. The value of $\mathrm{d}\sigma/\mathrm{d}t\ (t_0)$ has been obtained from the experimental fits of Barber et al. at low momentum transfers and in the energy range between 3.4 and 4.8 GeV (see Fig. 7 of [18]). We took $\mathrm{d}\sigma/\mathrm{d}t = (2.13 \pm 0.38)\,\mu\mathrm{b/GeV}^2\ \exp[\,(6.2 \pm 1.3)\,\mathrm{GeV}^{-2}\ t]$ and calculated its value at the minimum $|t_0|$ argument corresponding to the $K\overline{K}$ effective mass 1.042 GeV, which

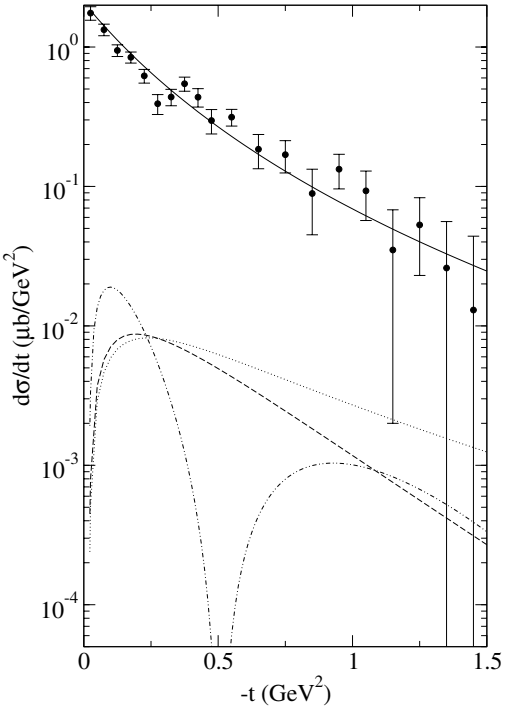

Fig. 2. Differential cross section at $E_\gamma = 4\,\text{GeV}$. The solid line shows the model t-distribution for the ϕ photoproduction, the dotted line is the P-wave contribution with $M = 0$ multiplied by the branching ratio of the ϕ decay into the K^+K^- pair. The dashed line is the S-wave part of the K^+K^- cross section calculated for normal ρ,ω propagators, while the double dotted-dashed line corresponds to the Regge propagators. Model parameters are given in Table 1. The data are from Fig. 6b of [18]

Table 1. Fitted values of model parameters for $E_\gamma = 4\,\text{GeV}$. Units of A and B are μb/GeV and μb/GeV^2, respectively

	Normal propagators	Regge propagators
ϕ_{00}	$122.3^\circ\,^{+22.6^\circ}_{-21.5^\circ}$	$74.5^\circ\,^{+29.7^\circ}_{-27.0^\circ}$
ϕ_{10}	$87.6^\circ\,^{+9.9^\circ}_{-11.1^\circ}$	$86.8^\circ\,^{+12.8^\circ}_{-23.1^\circ}$
C_{00}	0.33 ± 0.16	$0.72\,^{+0.42}_{-0.43}$
C_{10}	$0.44\,^{+0.16}_{-0.22}$	$0.37\,^{+0.18}_{-0.31}$
A	$6.65\,^{+0.22}_{-0.23}$	$6.67\,^{+0.22}_{-0.24}$
B	133.0 ± 11.9	133.1 ± 11.9
v_{10}	$(-12.2\,^{+6.6}_{-6.7})\times10^{-3}$	$(-11.3 \pm 6.5)\times10^{-3}$
v_{11}	$(-2.0 \pm 5.5)\times10^{-3}$	$(-1.2\,^{+5.5}_{-5.6})\times10^{-3}$
v_{20}	$(-7.8\,^{+8.9}_{-9.0})\times10^{-3}$	$(-6.5\,^{+8.9}_{-9.1})\times10^{-3}$

was the upper limit studied in [18]. Then the constant D_1 equals

$$D_1 = \left(\frac{\mathrm{d}\sigma/\mathrm{d}t\ (t_0)\ \mathrm{BR}}{\mathrm{Int}}\right)^{\frac{1}{2}}, \qquad (17)$$

where BR = 0.486 is the branching ratio for the ϕ decay into K^+K^- used in [18] and

$$\mathrm{Int} = \int_{M_1}^{M_2} \frac{\mathrm{d}\sigma^P}{\mathrm{d}t\ \mathrm{d}M_{K\overline{K}}}(D_1 = 1, t_0)\ \mathrm{d}M_{K\overline{K}}\,, \qquad (18)$$

M_1 being the lower effective mass limit 0.997 GeV and M_2 being the upper mass limit 1.042 GeV. In the above equation the unnormalized double differential cross section $\mathrm{d}\sigma^P/(\mathrm{d}t\ \mathrm{d}M_{K\overline{K}})$ corresponds to the P-wave amplitudes calculated at fixed t_0. A variation of the t_0 with the effective mass K^+K^- has been neglected in this narrow band of $M_{K\overline{K}}$.

As expected, the t-distribution is dominated by the helicity non-flip P-wave. The P_0-wave and the S-wave are kinematically suppressed at low t and are two orders of magnitude smaller than the dominant wave. After integration over t in the range up to $-t = 1.5\,\text{GeV}^2$ the total ϕ photoproduction cross section equals 0.449 μb and is in very good agreement with the measured value of (0.450 ± 0.019) μb presented in Table 1 of [18] for the photon energy range between 2.8 and 4.8 GeV. The K^+K^- part of the integrated P-wave cross section equals (0.218 ± 0.039) μb. In the model fits to the data, the decomposition of the total P-wave cross section in its parts corresponding to $M = 1$, $M = 0$ and $M = -1$ components depends to some extent on the contribution of the S-wave cross section and in particular on the choice of the type of propagators included in the S-wave amplitude. For normal ρ,ω propagators the integrated cross sections for the P_0-wave and the S-wave are equal to $(6.4^{+5.5}_{-4.8})$ nb and $(4.9^{+5.8}_{-3.6})$ nb, respectively. The corresponding numbers for the Regge propagators are $(4.7^{+5.7}_{-4.5})$ nb and $(4.3^{+6.6}_{-3.6})$ nb. The errors of the cross sections have been evaluated using the limits of the model parameters obtained from the fitting program MINUIT [27]. These numbers are smaller than our early estimates of the S-wave integrated cross sections written in [20]. One reason of this change is related to the presence of the S-wave form factor $\exp(B_S t)$ introduced in the previous section, and the second one comes from the diminution of the S-wave modulus obtained in the fitting procedure, which will be explained later.

3.2 Momentum transfer distributions and integrated cross sections at $E_\gamma = 5.65\,\text{GeV}$

The DESY data [17] have been taken at much lower momentum transfers than the Daresbury data [18]. The most precise data of Behrend et al. lie within the range $|t - t_{\min}| < 0.2\,\text{GeV}^2$. The average energy $E_\gamma = 5.65\,\text{GeV}$corresponds to the photon energy range between 4.6 and 6.7 GeV. The ϕ production differential cross section $\mathrm{d}\sigma/\mathrm{d}t$ can be fitted as $\mathrm{d}\sigma/\mathrm{d}t = n\ \exp(bt)$, where $n = (2.40 \pm 0.15)$ μb/GeV^2 and $b = (6.11 \pm 0.53)\,\text{GeV}^{-2}$ represents the average slope of $\mathrm{d}\sigma/\mathrm{d}t$ for the four upper energy bins given in Table 3 of [17]. Taking the appropriate t_0 value equal to $-0.0113\,\text{GeV}^2$ we calculate $\mathrm{d}\sigma/\mathrm{d}t\ (t_0) = 2.24$ μb/ GeV^2. Then we define the simple form of the t-dependent normalization factor at $E_\gamma = 5.65\,\text{GeV}$

$$F(t) = D_2\ \mathrm{e}^{\frac{1}{2}bt}\,, \qquad (19)$$

and use once again (17) and (18) to find a new constant D_2, taking into account that the ϕ branching ratio used in [17] was BR = 1/2.14, $M_1 = 1.01\,\text{GeV}$ and $M_2 = 1.03\,\text{GeV}$. The K^+K^- photoproduction cross section at $E_\gamma = 5.65\,\text{GeV}$ integrated over $|t|$ up to $0.2\,\text{GeV}^2$

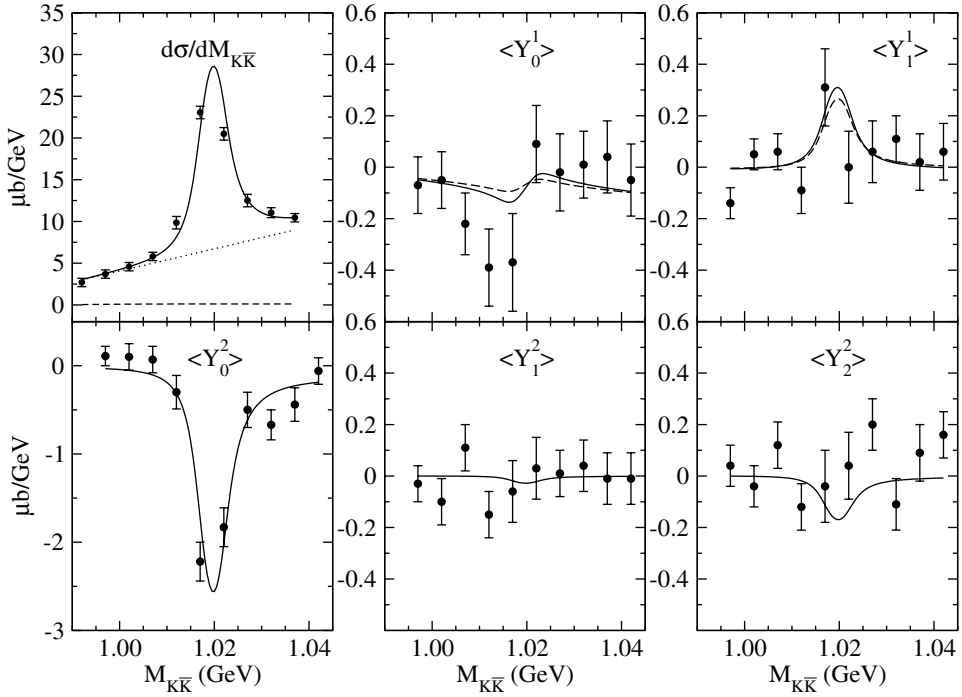

Fig. 3. K^+K^- mass spectrum and moments of angular distribution in the helicity frame for an incident photon energy of 4 GeV. Solid lines are results of model calculations for the normal ρ, ω propagators, while the dashed lines correspond to the Regge propagators. The dotted line shows the background contribution to the mass spectrum, while the short dashed line represents the S-wave part. The phenomenological parameters are given in Table 1. The data points are from [18]

is 120.5 nb. Its P_0- and S-wave parts are $(13.8^{+5.3}_{-4.7})$ nb and $(7.0^{+6.8}_{-4.4})$ nb for normal propagators and $(14.0^{+5.3}_{-4.8})$ nb and $(6.8^{+6.6}_{-4.3})$ nb for Regge propagators, respectively. Let us notice that the P_0- and S-wave cross sections are comparable and do not vary too much with energy, bearing in mind rather large errors. The S-wave cross section at 5.65 GeV is comparable in magnitude with the estimate of the upper limit (2.7 ± 1.5) nb quoted in [16,17]. We finally note that the total ϕ photoproduction cross section of (0.25 ± 0.2) μb, given in [16], corresponds to $M_{K\overline{K}}$ integrated over the range 1.0 GeV to 1.024 GeV. When integrated in this mass range our model gives 0.23 μb, in good agreement with the measurement.

3.3 K^+K^- mass distributions and moments at $E_\gamma = 4$ GeV

Next let us describe calculations of the K^+K^- differential cross section integrated over a certain range of the momentum transfer at fixed $M_{K\overline{K}}$ mass. We first discuss the results corresponding to $E_\gamma = 4$ GeV where the upper limit of $-t$ was 1.5 GeV^2. In Fig. 3 we show the results of the simultaneous fit to the K^+K^- effective mass distribution $\mathrm{d}\sigma/\mathrm{d}M_{K\overline{K}}$ in the mass range $0.992 < M_{K\overline{K}} < 1.037$ GeV and to the moments $\langle Y^L_M \rangle$ at $0.997\,\mathrm{GeV} < M_{K\overline{K}} < 1.042\,\mathrm{GeV}$. To account for a possibly large $\pi\pi$ experimental background in [18] we have introduced an additional linear term

$$\frac{\mathrm{d}\sigma_b}{\mathrm{d}M_{K\overline{K}}} = A + B(M_{K\overline{K}} - M_{\mathrm{av}})\,, \qquad (20)$$

where A and B are free parameters and $M_{\mathrm{av}} = (M_1 + M_2)/2$ is the average $K\overline{K}$ effective mass in the range chosen above. The parameters A and B will be fitted to the experimental data. The background cross section integrated over the mass range between M_1 and M_2 is equal to $A(M_2 - M_1)$. It is rather large, attaining a value of about 300 nb. Similarly we have added the background terms to three moments:

$$\langle Y^1_0 \rangle_b = v_{10} \frac{\mathrm{d}\sigma_b}{\mathrm{d}M_{K\overline{K}}}\,, \quad \langle Y^1_1 \rangle_b = v_{11} \frac{\mathrm{d}\sigma_b}{\mathrm{d}M_{K\overline{K}}}\,,$$
$$\langle Y^2_0 \rangle_b = v_{20} \frac{\mathrm{d}\sigma_b}{\mathrm{d}M_{K\overline{K}}}\,, \qquad (21)$$

where v_{10}, v_{11} and v_{20} are constants. The remaining two moments $\langle Y^2_1 \rangle$ and $\langle Y^2_2 \rangle$ have not been corrected for background, since their experimental values fluctuate around zero [18]. In the fits to the data a finite experimental resolution of the effective K^+K^- mass distribution was taken into account by choosing the effective ϕ width equal to 5.6 MeV according to the K^+K^- spectrum in Fig. 5 of [18]. The theoretical effective mass distribution and the moments have been smeared over the mass interval $\Delta M_{K\overline{K}} = 5$ MeV equal to the mass bin size. Both effects lead to a broadening of the ϕ resonance spectrum and to a widening of the structure of moments near the ϕ mass. The overall number of free parameters in our fit is 9 (or 7 if v_{11} and v_{20} are set to zero, which they are within errors). Table 1 presents the values of fitted model parameters in cases of normal and Regge propagators used in the S-wave amplitudes. The total number of experimental data is 60. We see in Fig. 3

that all the moments are well fitted including the moment $\langle Y_0^1\rangle$. One has the impression that the theoretical curve corresponding to this moment has a slightly too small amplitude near 1.015 GeV, but the χ^2 value for 10 data points is good: equal to 8. The S-wave cross section is small, almost invisible in comparison with the large peak corresponding to the ϕ resonance and the very important background which we attribute to an experimental misidentification of the $\pi\pi$ events as $K\overline{K}$ events. In our fits of the moments we have not assumed like in [18] that the nucleon non-flip S-wave amplitudes vanish. In fact, they do not vanish and become more important at higher values of t. Thus we have included the moment $\langle Y_1^1\rangle$ in our analysis without making the ad hoc assumption that it is zero from the beginning. We see in Fig. 3 that $\langle Y_1^1\rangle$ is in general non-zero and has some structure near 1.02 GeV related to the position of the maximum of the dominant P-wave. The experimental values of the moment $\langle Y_1^2\rangle$ are particularly small. In our model this moment is also small due to the large phase difference ϕ_{10} between the P-wave amplitudes with $M = 1$ and $M = 0$. This phase is close to 90° as seen in Table 1. The S-wave phase has also a large correction ϕ_{00}, which depends on the type of propagators used in the model. This phase is smaller for the Regge propagators since they are complex and vary with the momentum transfer. On the average the Regge propagators add about 50° to the phase of the S-wave. This increase is compensated by a decrease of ϕ_{00}.

Among the S-wave amplitudes, the proton spin non-flip components are the most important ones, although their dominance is not so strong as in the case of the P-wave. This feature of the S-wave amplitudes is related to an important contribution of the ρ exchange. The phase difference between the S-wave proton spin non-flip and the P_0-wave proton spin non-flip amplitudes is larger than 90° for the $M_{K\overline{K}}$ masses smaller than the ϕ mass and it becomes smaller than 90° on the right hand side of the ϕ resonance. This happens due to the rapid phase increase of the resonant P_0 amplitude. As a consequence of this phase variation the moment $\langle Y_0^1\rangle$ has a minimum to the left of the ϕ resonance position and the maximum to its right. Let us stress here that only this moment has been analyzed in [18] as a source of S–P-wave interference. We should remark, however, that the moment $\langle Y_1^1\rangle$ also depends sensitively on the S-wave amplitudes.

In addition to phases the fitting program provides us with the values of the moduli C_{00} and C_{10}. At 4 GeV both factors are smaller than 1, so the integrated cross sections for the S-wave and the P_0-wave are reduced in magnitude and their final numbers stay below 10 nb as already written.

3.4 K^+K^- mass distributions and moments at $E_\gamma = 5.65$ GeV

We turn to a discussion of the angular momentum structure at the average photon energy 5.65 GeV. The authors of [17] have presented in their Fig. 22 the so-called normalized moments of the spherical harmonics $\langle Y_M^L\rangle/\langle Y_0^0\rangle$ together with the unnormalized $K\overline{K}$ mass distribution representing the numbers of events per 10 MeV bin. We have attempted to make our own normalization of the above data in order to obtain the functional dependence of the moment $\langle Y_0^0\rangle$ which is equal to the differential cross section $\mathrm{d}\sigma/\mathrm{d}M_{K\overline{K}}$ divided by $(4\pi)^{1/2}$. We have integrated the ϕ production differential cross section $\mathrm{d}\sigma/\mathrm{d}t$ parameterized above as a simple exponential function in the $-t$ range up to 0.2 GeV^2 obtaining the value of (0.258 ± 0.020) μb. This value corresponds to the sum of 3927 ± 82 K^+K^- events in the $M_{K\overline{K}}$ range between 1.01 and 1.03 GeV. Taking into account the K^+K^- branching ratio reported as 1/2.14 in [17], we get the normalization constant equal to $(3.068 \pm 0.245) \cdot 10^{-5}$ μb/event. Knowing this constant one can calculate the moment $\langle Y_0^0\rangle$ and consequently the values of all other moments $\langle Y_M^L\rangle$ for L and M up to 2. Then we have performed a common fit to $\mathrm{d}\sigma/\mathrm{d}M_{K\overline{K}}$ and 5 moments $\langle Y_M^L\rangle$ for $M_{K\overline{K}}$ between 1.005 and 1.045 GeV, including fully the range of the $\phi(1020)$ resonance as well as a part of $M_{K\overline{K}}$ well above it. Here the width of the mass bins was 10 MeV. Unfortunately the value of the mass distribution $\mathrm{d}\sigma/\mathrm{d}M_{K\bar{K}}$ corresponding to the extreme experimental data point at 0.995 GeV was not given in [17], even though the $L \neq 0$ normalized moments were presented. For this reason we were unable to include this bin in our fit. The effective mass resolution reported in [17] was about 7 MeV and the effective ϕ width chosen in the analysis done by [16] was 8 MeV. We included the finite mass resolution by smearing our theoretical mass spectrum and moments over the 8.5 MeV range around each $M_{K\overline{K}}$ value. In the P-wave amplitudes the Breit–Wigner form of the ϕ spectrum was used with the ϕ mass equal to 1.0194 GeV and the width equal to 4.26 MeV. As at 4 GeV energy we have introduced a linear background term in the effective K^+K^- mass distribution and in the two moments:

$$\langle Y_0^2\rangle_b = \beta_{20}(M_{KK} - M_{\mathrm{th}})\,, \quad \langle Y_1^2\rangle_b = \beta_{21}(M_{KK} - M_{\mathrm{th}})\,, \tag{22}$$

where β_{20} and β_{21} are parameters, and M_{th} is the threshold mass of the $K\overline{K}$ system. Counting the four parameters in the two complex factors $C_{00}\ \exp(\mathrm{i}\phi_{00})$ and $C_{10}\ \exp(\mathrm{i}\phi_{10})$ which modify the S-wave and the P_0-wave amplitudes, and adding two background parameters A and B, we have altogether eight parameters to be fitted to the data at 5.65 GeV. The results of the fits are shown in Fig. 4 and the parameters are written in Table 2. Contrary to the previous case of $E_\gamma = 4$ GeV, the background cross section at 5.65 GeV is much smaller, less than 5 nb. The shape of the $K\overline{K}$ mass spectrum and the general behavior of the moments are well described by the model perhaps except for the two points of $\langle Y_0^2\rangle$ at 1.005 and 1.015 GeV. The values corresponding to these data points are *smaller* than −0.45. Let us notice that the *lowest* limit of $\langle Y_0^2\rangle/\langle Y_0^0\rangle$ equals $-1/\sqrt{5} \approx -0.45$ if one assumes that only S- and P-waves participate in the K^+K^- production process. Strictly speaking, this limit corresponds to the case in which the amplitudes P_+ dominate near the position of the $\phi(1020)$ resonance. Any admixture of the P_0-, P_-- or S-waves must increase the value of $\langle Y_0^2\rangle/\langle Y_0^0\rangle$ above $-1/\sqrt{5}$. A uniform background contribution would have the same effect. Thus, one is tempting to explain the low experimental values at 1.005 and 1.015 GeV

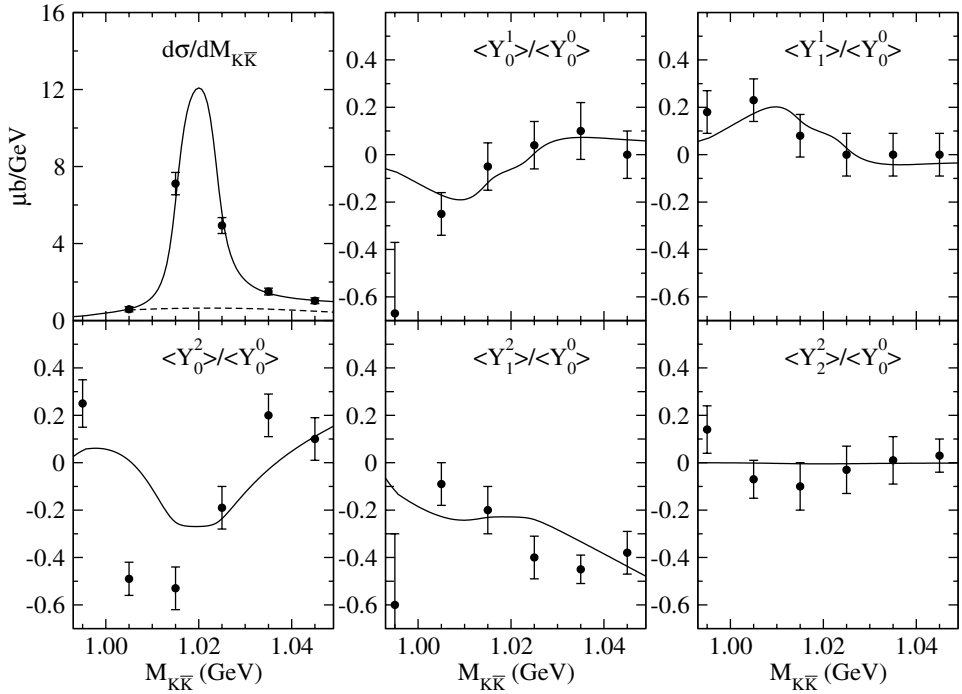

Fig. 4. K^+K^- mass distribution and normalized moments of the angular distribution in the helicity system for an incident photon energy of 5.65 GeV. The solid lines are results of model calculations; the dashed line is the S-wave contribution to the mass distribution. The phenomenological parameters are given in Table 3. The data points are from [17]

Table 2. The fitted values of model parameters for $E_\gamma = 5.65\,\text{GeV}$. Units of A are μb/GeV and B, β_{20} and β_{21} are in μb/GeV^2

	Normal propagators	Regge propagators
ϕ_{00}	$106.0^\circ\,^{+10.2^\circ}_{-16.2^\circ}$	$49.3^\circ\,^{+10.1^\circ}_{-16.0^\circ}$
ϕ_{10}	$11.4^\circ\,^{+17.3^\circ}_{-16.6^\circ}$	$13.0^\circ\,^{+17.2^\circ}_{-16.7^\circ}$
C_{00}	$1.06\,^{+0.43}_{-0.41}$	$1.53\,^{+0.61}_{-0.59}$
C_{10}	$1.59\,^{+0.28}_{-0.30}$	$1.60\,^{+0.28}_{-0.30}$
A	$0.23\,^{+0.21}_{-0.31}$	$0.24\,^{+0.21}_{-0.29}$
B	$7.14\,^{+4.81}_{-4.80}$	$7.22\,^{+4.82}_{-4.80}$
β_{20}	1.20 ± 0.45	1.19 ± 0.45
β_{21}	-1.98 ± 0.45	-1.98 ± 0.45

Table 3. Integrated cross sections in nb

Photon energy	4 GeV		5.65 GeV	
S-wave propagator	normal	Regge	normal	Regge
sum of all P-waves	218.4 ± 39.5		120.5 ± 9.4	
P_0-wave	$6.4^{+5.5}_{-4.8}$	$4.7^{+5.7}_{-4.5}$	$13.8^{+5.3}_{-4.7}$	$14.0^{+5.3}_{-4.8}$
S-wave	$4.9^{+5.8}_{-3.6}$	$4.3^{+6.6}_{-3.6}$	$7.0^{+6.8}_{-4.4}$	$6.8^{+6.6}_{-4.3}$
background	$299.4^{+10.0}_{-10.4}$	$300.0^{+10.0}_{-10.7}$	$4.5^{+4.3}_{-6.1}$	$4.7^{+4.2}_{-5.8}$
$\lvert t\rvert_{\max}$	1.5 GeV^2		0.2 GeV^2	
$M_{K\overline{K}}$ range	(0.997,1.042) GeV		(1.01,1.03) GeV	

by the presence of a background coming from higher waves, like D- or F-waves. Interestingly, slightly above the $\phi(1020)$ mass, there is a structure in the ratio of $\langle Y^4_0\rangle/\langle Y^0_0\rangle$ measured in [17]. This structure can be attributed to a D-wave or to interference of the P-wave with the F-wave. Both cases are, however, physically rather improbable, because near the $K\overline{K}$ threshold these waves should be strongly suppressed, and we do not know any D or F resonances located closely to 1 GeV. Let us also remark that the general shape of $\langle Y^2_0\rangle/\langle Y^0_0\rangle$ shown by the line in Fig. 4 is correct near the $K\overline{K}$ threshold since the extreme experimental point at 0.995 GeV lies above and not too far from the curve. In Fig. 4 we do not show a line corresponding to the small background to $\mathrm{d}\sigma/\mathrm{d}M_{K\overline{K}}$, since its magnitude is very close to the S-wave contribution shown in this figure.

Finally, in Table 3 we list the contributions of the individual waves to the $K\overline{K}$ photoproduction cross section at the two energies studied.

3.5 Model predictions at the energy upgraded Jefferson Laboratory

We have performed calculations of the K^+K^- mass spectrum and moments at $E_\gamma = 8\,\text{GeV}$ which will be a typical energy of the planned upgrade of the CEBAF accelerator operating at the Thomas Jefferson Laboratory. The results presented in Fig. 5 can be directly compared with Fig. 3 corresponding to the much lower energy of 4 GeV. The calculations have been performed for the ideal case in which there is no background and no phenomenological adjustment of the moduli and phases of the S- and P_0-waves, i.e., $\phi_{00} = \phi_{10} = 0$, $C_{00} = C_{10} = 1$. We have assumed that the K^+K^- mass resolution is equal to 5 MeV. The param-

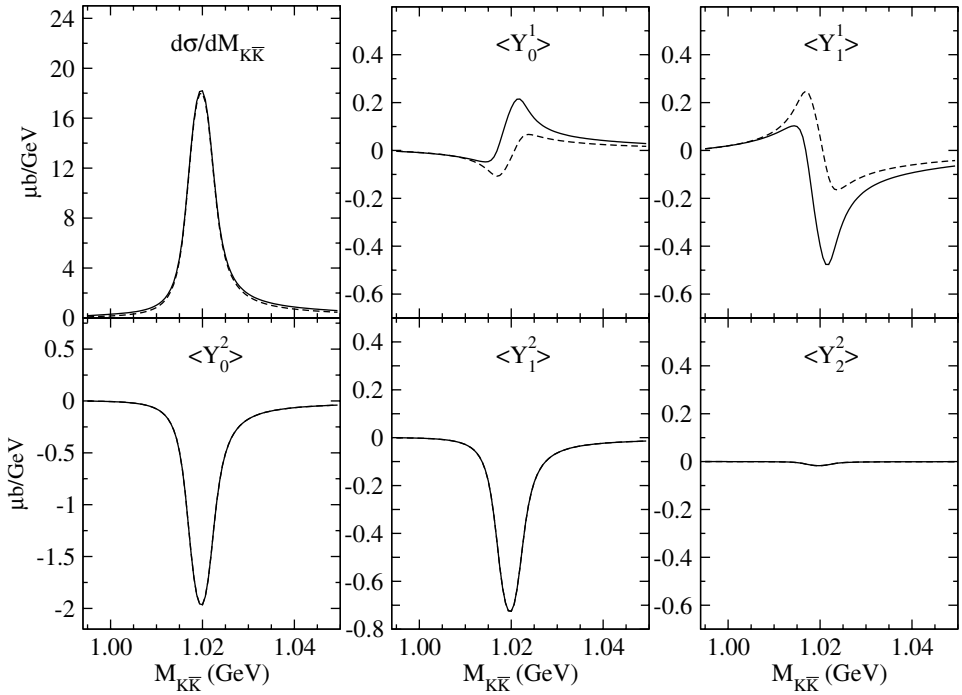

Fig. 5. K^+K^- mass spectrum and moments of angular distribution in the helicity frame for incident photon energy 8 GeV. Solid lines are results of model calculations for the normal ρ, ω propagators, while the dashed lines correspond to the Regge propagators in the S-wave amplitudes

eters of the $\phi(1020)$ meson, like the mass, width and the K^+K^- decay fraction, have been taken as 1019.456 MeV, 4.26 MeV and 0.492, respectively. The differential cross section at low t was parameterized as $\mathrm{d}\sigma/\mathrm{d}t = n\ \exp(bt)$, with $n = 2.53\,\mu\mathrm{b/GeV}^2$ and $b = 6.11\,\mathrm{GeV}^{-2}$. One can notice that the application of Regge propagators in the S-wave leads to smaller values of the S-wave cross section and to smaller amplitudes of the moments $\langle Y_0^1\rangle$ and $\langle Y_1^1\rangle$ sensitive to the interference between the S- and P-waves. Qualitatively we do not observe important differences in the behavior of the unnormalized moments between the photon energy of 5.65 and 8 GeV (let us recall here that Fig. 4 shows the ratios of $\langle Y_M^L\rangle/\langle Y_0^0\rangle$, not $\langle Y_M^L\rangle$).

The S-wave total cross sections integrated over the $M_{K\overline{K}}$ range between 1.01 and 1.03 GeV and in the $|t|$-range from 0.0054 up to 0.2 GeV^2 are equal to 6.9 nb and 3.0 nb for the normal and Regge propagators, respectively. The P-wave cross section integrated in the same ranges equals 141 nb while the corresponding P_0-cross section is equal to 6 nb.

4 Conclusions

In this paper we presented results of a theoretical analysis of the data on photoproduction of the K^+K^- pairs in the laboratory photon energy range E_γ between 2.8 and 6.7 GeV. In particular we mapped out the interference pattern between the S- and the P-wave due to the presence of the scalar $f_0(980)$, $a_0(980)$ and the vector $\phi(1020)$ resonances. In the analyses the S-wave was described by a model based on the dominance of the t-channel exchange process with the two-meson spectrum described in terms of the coupled channel meson–meson scattering S-matrix. The P-wave was described in terms of diffractive production of the ϕ resonance decaying into the K^+K^- system. The S-wave and the P-wave contain 4 and 12 independent amplitudes respectively and we included them all, while previous analyses made a severe truncation to a single amplitude in each wave. We have shown that amplitudes omitted in the analyses of [16, 18] corresponding to the proton helicity non-flip are large and cannot be ignored. In the previous analyses only the $\langle Y_{10}\rangle$ moment was taken into account and this led to a large variation in the estimate of the S-wave photoproduction cross section, between (2.7 ± 1.5) nb at $E_\gamma = 5.65$ GeV [16, 17] and (96.2 ± 20) nb at $E_\gamma = 4$ GeV [18]. In this paper we have considered all six moments appearing in the model with S- and P-waves which enabled us to isolate the S-wave production cross section from that of an incoherent background. This led to a significant, order of magnitude, reduction in the uncertainty in the S-wave production and reduced the value of the cross section at 4 GeV from 96 nb to approximately 5 nb, thus eliminating the discrepancy between the two measurements (also suggested in [18]). Thus we have found that the S-wave photoproduction cross section integrated over the ϕ resonance region is between 4 and 7 nb for the two photon energies 4 and 5.65 GeV. The cross section of the photon helicity flip P_0-wave, which interferes with the S-wave is found to be somewhat larger than the S-wave cross section, in the range between 5 and 14 nb. New more precise measurements of the $K\overline{K}$ photoproduction with a

simultaneous determination of the $\pi\pi$ cross section in the $\pi\pi$ effective mass region near 1 GeV could provide new insight into the still controversial nature of the scalar mesons $f_0(980)$ and $a_0(980)$.

Acknowledgements. We thank Chueng-Ryong Ji and Robert Kamiński for their collaboration on the S-wave photoproduction and for an exchange of ideas on the P-wave amplitudes in the early stage of this work. One of us (L. L.) would like to thank Maria Różańska and Jacek Turnau for enlightening discussions on the analysis of experimental data. This work was supported in part (A. P. S.) by the US Department of Energy grant under contract DE-FG0287ER40365.

References

1. C. Amsler, Rev. Mod. Phys. **70**, 1293 (1998)
2. F. Antinori et al., Phys. Lett. B **353**, 589 (1995)
3. D. Barberis et al., Phys. Lett. B **413**, 217 (1997); B **453**, 316 (1999)
4. J.Z. Bai et al., Phys. Rev. Lett. **77**, 3959 (1996); D.V. Bugg et al., Phys. Lett. B **353**, 378 (1995)
5. G.S. Adams et al., Phys. Rev. Lett. **81**, 5760 (1998); E.I. Ivanov et al., Phys. Rev. Lett. **86**, 3977 (2001)
6. A.R. Dzierba et al., Phys. Rev. D **67**, 094015 (2003)
7. A.P. Szczepaniak, M. Swat, A.R. Dzierba S. Teige, hep-ph/0304095, to appear in Phys. Rev. Lett.
8. J.A. Oller, E. Oset, J.R. Pelaez, Phys. Rev. D **59**, 074001 (1999), Erratum D **60**, 099906 (1999); J.A. Oller, E. Oset, Phys. Rev. D **60**, 074023 (1999)
9. R. Kamiński, L. Leśniak, J.P. Maillet, Phys. Rev. D **50**, 3145 (1994); R. Kamiński, L. Leśniak, B. Loiseau, Eur. Phys. J. C **9**, 141 (1999)
10. M.A. Pichowsky, A.P. Szczepaniak, J.T. Londergan, Phys. Rev. D **64**, 036009 (2001)
11. G. Janssen, B.C. Pearce, K. Holinde, J. Speth, Phys. Rev. D **52**, 2690 (1995)
12. N. Isgur, V.A. Kostelecky, A.P. Szczepaniak, Phys. Lett. B **515**, 333 (2001)
13. L. Gorlich et al., Nucl. Phys. B **174**, 16 (1980); W. Wetzel et al., Nucl. Phys. B **115**, 208 (1976)
14. M. Atkinson et al., Z. Phys. C **27**, 233 (1985); D. Aston et al., Nucl. Phys. B **172**, 1 (1980)
15. M.A. Pichowsky, T.S.H. Lee, Phys. Rev. D **56**, 1644 (1997)
16. D.C. Fries et al., Nucl. Phys. B **143**, 408 (1978)
17. H.-J. Behrend et al., Nucl. Phys. B **144**, 22 (1978)
18. D.P. Barber et al., Z. Phys. C **12**, 1 (1982)
19. J.D. Jackson, Nuovo Cim. **34**, 1644 (1964)
20. C.- R. Ji, R. Kamiński, L. Leśniak, A.P. Szczepaniak, R. Williams, Phys. Rev. C **58**, 1205 (1998)
21. L. Leśniak, A.P. Szczepaniak, Acta. Phys. Pol. B **34**, 3389 (2003)
22. R. Kamiński, L. Leśniak, B. Loiseau, Phys. Lett. B **413**, 130 (1997)
23. R. Kamiński, L. Leśniak, K. Rybicki, Z. Phys. C **74**, 79 (1997)
24. L. Leśniak, Acta. Phys. Pol. B **27**, 1835 (1996)
25. A. Furman, L. Leśniak, Phys. Lett. B **538**, 266 (2002); A. Furman, L. Leśniak, Nucl. Phys. B (Proc. Suppl.) **121**, 127 (2003)
26. A. Donnachie, P.V. Landshoff, Phys. Lett. B **348**, 213 (1995)
27. F. James, M. Roos, Comp. Phys. Commun. **10**, 343 (1975)